JACS
JOURNAL OF THE AMERICAN CHEMICAL SOCIETY
Article
pubs.acs.org/JACS

Principles of Sustained Enzymatic Hydrogen Oxidation in the Presence of Oxygen − The Crucial Influence of High Potential Fe−S Clusters in the Electron Relay of [NiFe]-Hydrogenases

Rhiannon M. Evans,[†] Alison Parkin,[†] Maxie M. Roessler,[†,‡] Bonnie J. Murphy,[†] Hope Adamson,[†] Michael J. Lukey,[†] Frank Sargent,[§] Anne Volbeda,[∥] Juan C. Fontecilla-Camps,[∥] and Fraser A. Armstrong*[,†,‡]

[†]Department of Chemistry and [‡]Centre for Advanced Electron Spin Resonance, South Parks Road, OX1 3QR Oxford, U.K.

[§]College of Life Sciences, University of Dundee, Dow Street, Dundee DD1 5EH, Scotland, U.K.

[∥]Metalloproteins Unit, Institut de Biologie Structurale J.-P. Ebel, Commissariat à l'Energie Atomique-Centre National de la Recherche Scientifique-Université Joseph Fourier, 41 Rue Jules Horowitz, 38027 Grenoble, France

Supporting Information

ABSTRACT: "Hyd-1", produced by *Escherichia coli*, exemplifies a special class of [NiFe]-hydrogenase that can sustain high catalytic H_2 oxidation activity in the presence of O_2—an intruder that normally incapacitates the sulfur- and electron-rich active site. The mechanism of "O_2 tolerance" involves a critical role for the Fe−S clusters of the electron relay, which is to ensure the availability—for immediate transfer back to the active site—of all of the electrons required to reduce an attacking O_2 molecule completely to harmless H_2O. The unique [4Fe-3S] cluster proximal to the active site is crucial because it can rapidly transfer two of the electrons needed. Here we investigate and establish the equally crucial role of the high potential medial [3Fe-4S] cluster, located >20 Å from the active site. A variant, P242C, in which the medial [3Fe-4S] cluster is replaced by a [4Fe-4S] cluster, is unable to sustain steady-state H_2 oxidation activity in 1% O_2. The [3Fe-4S] cluster is essential only for the first stage of complete O_2 reduction, ensuring the supply of all three electrons needed to form the oxidized inactive state "Ni−B" or "Ready" (Ni(III)−OH). Potentiometric titrations show that Ni−B is easily reduced ($E_m \approx +0.1$ V at pH 6.0); this final stage of the O_2-tolerance mechanism regenerates active enzyme, effectively completing a competitive four-electron oxidase cycle and is fast regardless of alterations at the proximal or medial clusters. As a consequence of all these factors, the enzyme's response to O_2, viewed by its electrocatalytic activity in protein film electrochemistry (PFE) experiments, is merely to exhibit attenuated steady-state H_2 oxidation activity; thus, O_2 behaves like a reversible inhibitor rather than an agent that effectively causes irreversible inactivation. The data consolidate a rich picture of the versatile role of Fe−S clusters in electron relays and suggest that Hyd-1 can function as a proficient hydrogen oxidase.

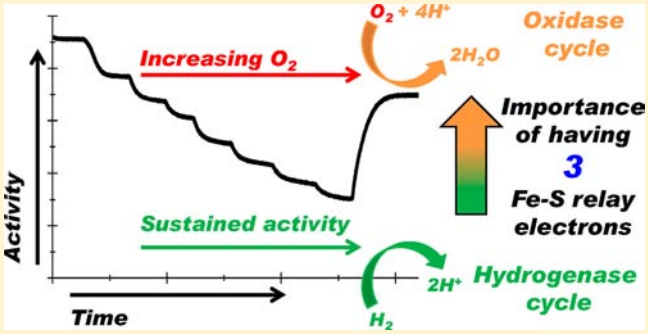

INTRODUCTION

Hydrogenase Classification. Hydrogenases, the two major classes of which are known as "[FeFe]" or "[NiFe]" according to the first-row transition metals in their buried active sites, catalyze the reversible oxidation of H_2 in microbes ($H_2 \rightleftharpoons 2H^+ + 2e^-$) at rates comparable to Pt.[1,2] *Escherichia coli* produces two [NiFe] uptake (respiratory) Class I[3] periplasmic membrane-bound hydrogenases (MBH), known as "Hyd-1" and "Hyd-2".[4−7] Analyzed by protein film electrochemistry (PFE),[8−10] Hyd-1 and Hyd-2 differ in terms of their relative activities for H_2 oxidation or production, and in their H_2 oxidation activity in the presence of O_2; specifically, Hyd-1 is "oxygen tolerant", that is, capable of continuous H_2 oxidation during prolonged O_2 exposure. Hyd-2 is "oxygen sensitive" and is inactivated quickly by trace concentrations of O_2.[8]

Defining Oxygen Tolerance. Figure 1 shows the aims of this work in the context of the general model for O_2 tolerance. There is increasing evidence that O_2 tolerance in membrane-bound [NiFe]-hydrogenases is linked to facilitating immediate recovery of active enzyme upon reaction with O_2[11] rather than avoiding this reaction in the first place by restricting O_2 access to the active site, for example, as seen in regulatory hydrogenases.[12−17] An important factor appears to be the availability of electrons to reduce the attacking O_2 molecule *directly* to water (see black box). If this demanding four-electron/multiproton reaction is not achieved in its entirety, reactive oxygen species become trapped within the active site

Received: November 9, 2012
Published: February 11, 2013

   dx.doi.org/10.1021/ja311055d | J. Am. Chem. Soc. 2013, 135, 2694−2707

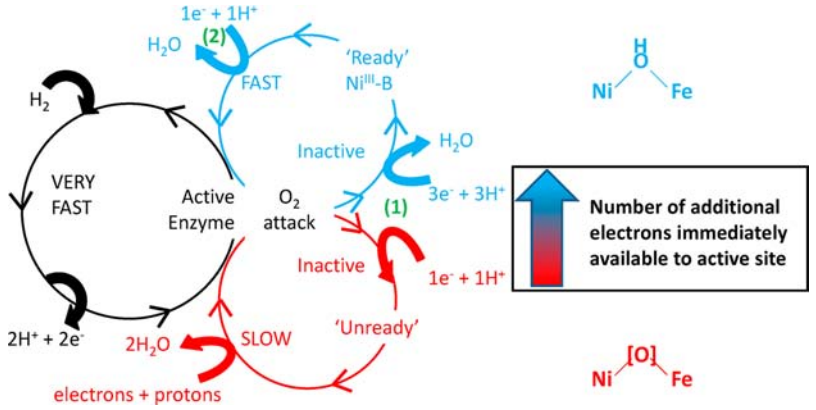

Figure 1. General model of oxygen tolerance adapted from Cracknell et al., 2009. Enzyme actively oxidizing H_2 is depicted in the black cycle. When O_2 attacks the active enzyme there are two pathways to inactive states, namely formation of "Ready" (blue, bridging hydroxide) and formation of states known as "Unready" (red, partially reduced oxygen species are drawn as [O]). The determining factor as to which path is taken, depicted in the black box, is the number of additional electrons (from the relay) that are immediately available to the active site when O_2 attacks. At least one electron is always available from the active site itself. The aims of this work are divided into understanding: (1) the first stage in dealing with O_2 attack, ensuring the formation of Ni–B, and (2) the second stage, in which Ni–B (a Ni(III)–OH species) is reduced back to active enzyme, which requires a further electron from the relay.

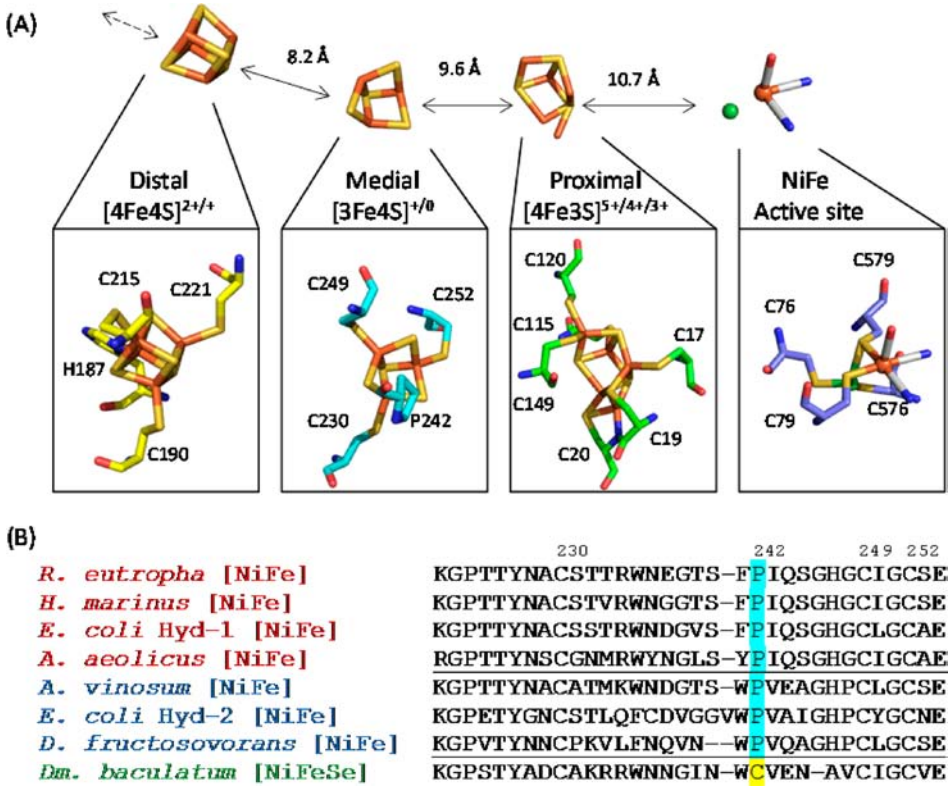

Figure 2. Spatial arrangement and ligating residues of the distal, medial and proximal Fe–S clusters relative to the active site in *E. coli* Hyd-1 (A, PDB: 3USE), and a sequence alignment (B) carried out using Clustal W.[73] Double headed arrows in (A) refer to the edge-to-edge distance between the redox centers. For the sequence alignment, only the section of interest with respect to the medial cluster ligation is included for various O_2-tolerant (red) and standard (blue) [NiFe]-hydrogenases, and [NiFeSe]-hydrogenase from *Dm. baculatum* (green). *R. eutropha* = *Ralstonia eutropha*, *H. marinus* = *Hydrogenovibrio marinus*, *E. coli* Hyd-1 = *Escherichia coli* Hydrogenase-1, *A. aeolicus* = *Aquifex aeolicus*, *A. vinosum* = *Allochromatium vinosum*, *E. coli* Hyd-2 = *Escherichia coli* Hydrogenase-2, *D. fructosovorans* = *Desulfovibrio fructosovorans*, *Dm. baculatum* = *Desulfomicrobium baculatum*. The cysteine residue which ligates the medial [4Fe-4S] cluster in the [NiFeSe]-hydrogenase and corresponding proline residues in [NiFe]-hydrogenases are highlighted in yellow and cyan, respectively. The three other ligating cysteines are also numbered. *E. coli* Hyd-1 sequence numbering is used.

resulting in various oxygenated species collectively represented as [O] (red cycle).[11,18,19] Assignments for [O] include peroxido-Ni(III) species[18−20] and oxidized cysteine.[9,19−22] The [O]–modified forms, which include a spectroscopically characterized state known as Ni–A, are referred to as "Unready" because their reductive reactivation is orders of magnitude slower than for an alternative oxidized inactive state known as Ni–B or "Ready".[9,18] "Ready", which can be regarded

dx.doi.org/10.1021/ja311055d | J. Am. Chem. Soc. 2013, 135, 2694−2707

as a resting state of the enzyme, is the harmless product of complete four-electron reduction of O_2, in which a hydroxide ligand remains bound to Ni(III) at the active site (blue cycle).[19,23] Oxidation by O_2 may give a mixture of Ready and Unready states, as seen in some aerobically purified enzymes;[8,9,24] additionally, Ni−B is formed under anaerobic oxidizing conditions.[8,25−28] Both the reactivation of Ni−B and its formation by the anaerobic route require hydrophilic channels for transporting water (or OH^-).[29]

Avoiding Slow-recovering O_2-inhibited States. According to the model in Figure 1, sustained catalytic oxidation of H_2 in the presence of O_2 requires avoiding formation of Unready states and ensuring that Ni−B is always formed instead.[11] This requires fast delivery of sufficient electrons to the active site to completely reduce the attacking O_2 and form Ni−B. Assuming that the most oxidized catalytic intermediate is a Ni(II) species known as Ni−SI (SI = EPR, electron paramagnetic resonance "silent") some simple sums predict what is required to reduce O_2 and form Ni−B (see (1) Figure 1). First, if O_2 attacks the active site at the level of Ni−SI, which is one electron more reduced than Ni−B, then three further electrons are required. Second, if O_2 attacks at the level of Ni−C, a Ni(III)-hydride species (formally two electrons more reduced than Ni−B) or an equivalent Ni(I) species without a hydride (Ni−L) then two electrons can be supplied from the hydride or Ni(I), and only two further electrons are required. Third, an attack by O_2 at the level of Ni−R (an IR (infra-red)-detectable Ni(II)-hydride species that is three electrons more reduced than Ni−B[30,31]) would require only one further electron. Following the formation of Ni−B, reactivation to active enzyme should require one electron (see (2) in Figure 1) which reduces Ni(III) to Ni(II) to generate a species at the oxidation level of Ni−SI, repaying the electron "borrowed" from the Ni when O_2 attacks. All these additional electrons must be provided by the Fe−S clusters that form a relay through the small subunit, electronically linking the active site in the large subunit to the natural redox partner at the bacterial membrane. The Fe−S clusters of Hyd-1 (Figure 2A) are named according to their position relative to the active site.

The Fe−S Relay in Hyd-1: the Proximal Cluster. The importance of the unusual proximal [4Fe-3S] cluster in conferring O_2 tolerance has been demonstrated through site-directed mutagenesis experiments on Hyd-1[9] and the O_2-tolerant MBH from *Ralstonia eutropha* H16 (*Re*-MBH).[32] The proximal cluster in these O_2-tolerent hydrogenases is ligated by six cysteines rather than the usual four. Supernumerary cysteine residues 19 and 120 (Figure 2A) were systematically exchanged for glycines, the corresponding residues found in standard [NiFe]-hydrogenases, and it was concluded that C19 (providing a side chain sulfur that partially replaces an inorganic core sulfide of the standard-like $[4Fe\text{-}4S](cys)_4$ cubane) is critical for O_2 tolerance.[9,32] Crystal structures of three O_2-tolerant [NiFe]-hydrogenases have been solved and the $[4Fe\text{-}3S](cys)_6$ proximal cluster is highly conserved.[29,33,34] More recently, HYSCORE experiments have been performed on a Hyd-1 medial cluster variant (see later) providing further insight into the proximal cluster's unique role.[35] The proximal cluster is able to undergo two sequential redox transitions: $[4Fe\text{-}3S]^{3+} \rightleftharpoons [4Fe\text{-}3S]^{4+} \rightleftharpoons [4Fe\text{-}3S]^{5+}$, the latter super-oxidized state having an unusual Fe−N(amide) bond that stabilizes a valence-localized Fe^{3+} subsite.[34,35] Acting alone, the proximal cluster can therefore deliver *two* electrons to the active site when O_2 attacks; the second electron transfer being coupled to amide deprotonation, thus maintaining local electroneutrality and avoiding an insurmountable Coulombic cost.[34,36] As we enumerated above, one more electron from the relay is then needed in order to ensure that Ni−B is formed regardless of the initial state of the active site when O_2 attacks, and our attention is thus directed to the medial Fe−S cluster.

The Fe−S Relay in Hyd-1: the Medial Cluster. The majority of Class I [NiFe]-hydrogenases have a [3Fe-4S] cluster in the medial position. The reduction potentials of $[3Fe\text{-}4S]^{+/0}$ clusters are more positive than their $[4Fe\text{-}4S]^{2+/+}$ counterparts.[37] Additionally, the reduction potential of the medial $[3Fe\text{-}4S]^{+/0}$ cluster in O_2-tolerant Hyd-1 (190 ± 30 mV at pH 6.0, or 215 ± 10 mV at pH 6.0 in the O_2-sensitive Hyd-1 C19G/C120G variant[35]) are considerably higher than that found in standard [NiFe]-hydrogenases, for example, *Desulfovibrio fructosovorans* (+65 mV at pH 8.0),[38] or *D. gigas* (−70 mV at pH 7).[39] Following early experiments in which the medial [3Fe-4S] cluster in the standard [NiFe]-hydrogenase from *D. fructosovorans* was mutated to a [4Fe-4S] cluster, thereby lowering the reduction potential to −250 mV (a decrease of 315 mV)[38] we recently carried out the equivalent mutation in Hyd-1; By changing the conserved proline-242 (see Figure 2B) to a cysteine, equivalent to the residue present in the Class I [NiFeSe]-hydrogenase from *Desulfomicrobium baculatum*, we "magnetically silenced" the medial cluster in its oxidized state, thus enabling us to resolve some of the complex EPR features of this enzyme using HYSCORE.[35]

Using the P242C mutation alone and in combination with C19G/C120G mutations at the proximal cluster[9] we now test the hypothesis that, by having a higher reduction potential than a [4Fe-4S] cluster[37] and thus being much more likely to have a electron bound and able to transfer when required, a [3Fe-4S] cluster in the medial position is important for conferring O_2 tolerance.

Our Aim. Protein film electrochemistry allows direct control of the oxidation states of the redox-active centers of an enzyme through the electrode potential, while the activity is simultaneously recorded as current.[18,40] We have used PFE to compare, in detail, the H_2 oxidation activities of native Hyd-1 and variants P242C, C19G/C120G and C19G/C120G/P242C in the presence and absence of O_2 to establish conclusively, that the importance of these clusters in O_2 tolerance lies in ensuring that O_2 attack results exclusively in the formation of Ni−B. We investigate the rates and potentials associated with Ni−B formation and reduction for variants altered at the medial or proximal clusters, and determine the number of electrons required to return to the catalytic cycle. The reduction potential of Ni−B is determined independently by EPR-based redox titrations. Our results demonstrate that the high-potential medial cluster[35] is essential for ensuring the exclusive formation Ni−B upon O_2 attack—a feature that allows sustained H_2 oxidation activity to occur at significant steady-state levels when O_2 is present. We also provide insight into the rate of catalytic four-electron O_2 reduction (oxidase activity) that must occur with high fidelity in O_2-tolerant hydrogenases.

MATERIALS AND METHODS

Molecular Biology. Details of all cloning steps carried out to produce the P242C, C19G/C120G and C19G/C120G/P242C Hyd-1 variants used in this study have been described previously.[9,35]

Expression of HyaA and Purification of Gene Products. Native and variant Hyd-1 enzymes were produced from MC4100[41]-derived *E. coli* K-12 strain FTH004[42] (or the appropriate variant strain

Table 1. X-Ray Data Collection and Refinement Statistics

crystal	1	1	1	2	2	3	3
data set:	1a	1b	1c	2a	2b	3a	3b
enzyme	native	native	native	P242C	P242C	P242C	P242C
detector	ADSC	ADSC	ADSC	Pilatus	Pilatus	Pilatus	Pilatus
λ (Å)	1.73470	1.74196	1.48164	0.95373	1.74135	0.97857	1.73890
N_{hkl}	73740	73840	128783	45793	28356	45094	32172
d_{max} (Å)	2.30	2.30	1.90	3.80	4.44	3.75	4.20
R_{sym} (%)	6.7	9.8	7.0	18.0	19.5	12.6	16.3
$\langle I/\sigma_I \rangle$	15.6	15.3	14.9	4.7	4.8	8.8	5.6
completeness (%)	97.2	97.3	96.7	98.8	98.0	99.9	99.6
refinement:							
resolution (Å)			15.0−1.9	25.0−3.8		20.0−3.75	
number of atoms							
R_{model} (%)			14.7	28.9		26.8	
R_{free} (%)			17.4	30.8		28.9	
σ_{bond} (Å)			0.011	0.009		0.011	
σ_{angle} (°)			1.2	1.1		1.2	

with the desired site-directed mutation(s)) carrying an engineered *hyaABCDEF* operon encoding a modified HyaA protein bearing a His_6 affinity tag at its extreme C terminus. Purification steps were followed as previously published,[8,9] except that 0.02% (w/v) *n*-dodecyl-*β*-D-maltoside (DDM) was replaced with 0.02% (w/v) Triton X-100.

Protein Film Electrochemistry. Protein film electrochemistry experiments were carried out in an anaerobic glovebox (MBraun or Glove Box Technology) with a N_2 atmosphere (O_2 < 2 ppm). Electrochemical measurements were made with an Autolab potentiostat (PGSTAT128N) controlled using Nova software (EcoChemie). A pyrolytic graphite "edge" (PGE) rotating disk electrode (RDE, of geometric surface area 0.03 cm^2) constructed in house[43] was the working electrode. The working electrode was controlled by an electrode rotator (EcoChemie or EG&G) and rotated at a constant speed (ω = 1000−4500 rpm depending on experimental requirements) to ensure rapid delivery of substrate to, and removal of product from, the electrode surface. This setup was used in conjunction with a thermostatted, gastight glass electrochemical cell that fitted snugly against the electrode rotator housing. Precise gas mixtures (BOC gases) were created using mass flow controllers (Sierra Instruments). The reference electrode (saturated calomel electrode, SCE) was housed in a nonisothermal side arm containing 0.10 M NaCl and connected to the main cell compartment by a Luggin capillary. Platinum wire was used as the counter electrode. The reference potential was converted to the standard hydrogen electrode (SHE) scale using the correction $E_{SHE} = E_{SCE} + 0.241$ V at 25 °C.[44] All potentials are quoted vs SHE. All electrochemical experiments were performed using a mixed buffer system,[26] adjusted to the desired pH at the working temperature for the experiment in question. All solutions were made with purified water (Millipore, 18 MΩ cm).

Each enzyme "film" was prepared in the same way: the PGE electrode was abraded using P400 Tufbak Durite sandpaper and wiped with cotton wool to remove any excess carbon. The surface of the electrode was then "spotted" with enzyme (~0.5−1 μL at 10−100 μM) and allowed to soak for ~30 s before holding under a stream of purified water to remove excess enzyme. Prior to each experiment, the enzyme film was reductively "activated" by poising the potential at −0.56 V for 300 s then monitoring H_2 oxidation activity at −0.06 V for 100 s. These potential steps were repeated until H_2 oxidation activity stabilized.

Crystallographic Analyses. Three different crystals were used to study the effect of the P242C mutation on the enzyme structure (Table 1). An orthorhombic form (crystal 1, space group $P2_12_12_1$ with cell dimensions a = 94.0 Å, b = 97.9 Å and c = 182.9 Å) was obtained from as-isolated native Hyd-1 using the conditions described previously.[34] Starting from the second major peak that was obtained for the preparation of the P242C variant after a Superdex200 gel filtration step, and following a final hydroxyapatite chromatography step, a different orthorhombic form was obtained (crystals 2 and 3, space group $P2_12_12_1$ with cell dimensions a = 130.8, b = 165.2, c = 214.3 Å and a = 124.7, b = 164.6, c = 210.6 Å, respectively). The crystallization conditions for the variant required a significantly higher protein concentration of 8 to 10 mg/mL, instead of the 2 to 5 mg/mL used for native Hyd-1. Crystal 2 was obtained at pH 5.3 using 16% PEG 4000 as precipitating agent in 100 mM sodium acetate (CH_3COONa), 200 mM ammonium acetate (CH_3COONH_4), 100 mM NaCl, 1 mM dithiothreitol (DDT) and 0.02% DDM. Crystal 3 was obtained at pH 8.2, using 16% PEG 3350 in 100 mM Tris HCl, 200 mM Li_2SO_4, 100 mM NaCl, 1 mM DTT and 0.02% DDM. All crystals were grown in an anaerobic glovebox and flash-cooled in liquid propane.[45]

X-ray diffraction intensity data were collected on beamline ID23−1 of the European Synchrotron Radiation Facility (crystal 1), beamline Proxima 1 of the SOLEIL synchrotron (crystal 2) and beamline X06SA of the Swiss Light Source (crystal 3). The crystals were kept under a cold N_2 stream at approximately 100 K. Data were indexed, integrated, scaled and converted to structure factor amplitudes (F_{obs}) with the XDS package.[46] Calculated structure factor amplitudes (F_{calc}) and phases were obtained from the molecular replacement solution of the structures with Phaser,[47] using the 1.47 Å resolution atomic model of the dimeric H_2-reduced form of native Hyd-1[34] as search model. The new orthorhombic form obtained for the variant (crystals 2 and 3) has two $(SL)_2$ dimers in the asymmetric unit, S and L denoting the small and large hydrogenase subunits respectively. Taking advantage of the presence of four hydrogenase copies in the asymmetric unit, 4-fold averaged electron density maps were used to model the P242C variant structure with COOT.[48] After rigid body refinement of the individual hydrogenase subunits, overall anisotropic movements of the $(SL)_2$ core structures were modeled with TLS refinement using Refmac.[49] In addition, tight noncrystallographic symmetry restraints were applied for the refinement of individual atomic positions (xyz) and isotropic temperature factors with the same program. Data sets of the same crystal collected at different X-ray wavelengths (λ) were scaled together with the scaleit program of the CCP4 package.[50] Data collected close to the Fe absorption edge, at $\lambda \approx 1.737$ Å for the inflection point (where the real component of f_{Fe}, the atomic scattering factor of Fe, is minimal) and at $\lambda \approx 1.742$ Å at the absorption maximum (where the imaginary component of f_{Fe} is maximal) were instrumental to probe the presence or absence of iron, using figure of merit (m) weighted anomalous difference (Δanom) and dispersive difference ($\Delta\lambda$) maps, along with $mF_{obs} - F_{calc}$ and $2mF_{obs} - DF_{calc}$ electron-density maps.[51] Data and refinement statistics are given in Table 1.

EPR Sample Preparation and Measurements. All EPR samples result from "as-isolated"[52] enzyme titrated to the desired potential under Ar with substoichiometric quantities of potassium ferricyanide

or sodium dithionite, following the addition of mediators (1,2-naphthoquinone, phenazine methosulfate, indigotetrasulfonate, 2-hydroxyl-1,4-naphthoquinone, methyl and benzyl viologen, each at a final concentration of 40 μM).[9,35] All samples were prepared in high-precision EPR tubes (Wilmad 714-PQ-7). The method of Bradford[53] was used to estimate the total protein concentration spectroscopically using a Perkin-Elmer Lamda 19 spectrophotometer, with bovine serum albumin as standard (Sigma Aldrich). Potentiometric EPR titrations ("Nernst plots") were constructed as described previously.[35] Continuous-wave EPR measurements were conducted on an X-band (9.1−9.9 GHz) Bruker EMX spectrometer (Bruker BioSpin GmbH, Germany) with an X-band superhigh sensitivity probehead (Bruker). Background spectra of the empty resonator were recorded under identical conditions and subtracted from the EPR spectrum of each enzyme sample. The field was calibrated at room temperature using 2,2-diphenyl-1-picrylhydrazyl as an external standard (g = 2.0036).

RESULTS

Structural Integrity of Variants. *Crystallographic Evidence for Cluster Conversion.* The new crystal form obtained for the P242C variant provided data to only medium resolution (Table 1), presumably due to the presence of partially disordered cytochrome *b*, which is not modeled here. In order to probe the presence of iron, difference (Δanom) and dispersive difference ($\Delta\lambda$) maps were compared at 4.5 Å resolution for native Hyd-1 and P242C (Figure 3) using two-

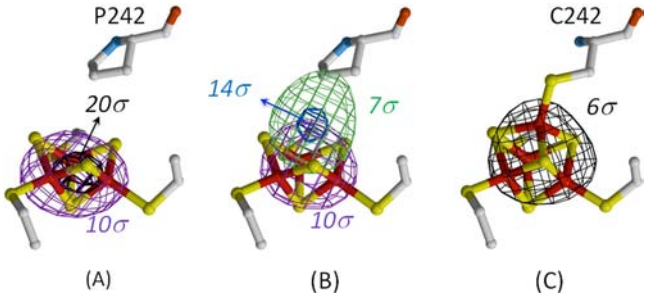

Figure 3. Crystallographic evidence for cluster conversion. Comparison of anomalous (Δanom) and dispersive difference ($\Delta\lambda$) maps for: (A) native Hyd-1 and (B) and (C) its P242C variant. The used X-ray wavelengths for the Δanom maps, shown as a purple grid, are 1.74196 and 1.74135 Å in (A) and (B), respectively. Black grids depict Fλ1−Fλ2 maps. The latter were calculated using X-ray wavelengths of λ1 = 1.48164 Å and λ2 = 1.73470 Å for native enzyme (A) and λ1 = 0.97857 Å and λ2 = 1.73890 Å for the variant (C). In addition, a 4-fold averaged omit ($mF_{obs} - F_{calc}$) map is shown in green and blue in (B). This map was calculated with phase information from a model with a proline (P242) and a [3Fe-4S] cluster. Contour levels are indicated in σ-units (in italics) in the given map colors, 1σ corresponding to the root-mean-square value of each map.

and four-fold density averaging, respectively. For P242C, phase information was used from the H_2-reduced native Hyd-1 model, excluding all solvent molecules, after its molecular replacement into the new crystal form and additional rigid body refinement. During this procedure the internal structure of the hydrogenase subunits did not change. The Fe−S clusters behave as "super-atoms" at 4.5 Å resolution, the peak density of which corresponds to the center of gravity of the individual Fe atoms. This is illustrated in Figure 3A for the native [3Fe-4S] cluster. As other metals would not give a significant peak in the ($\Delta\lambda$) map calculated from X-ray data collected at 1.48164 Å and 1.73470 Å, this figure further confirms the presence of three Fe atoms in the native cluster. For P242C, the peak density in both the Δanom and ($\Delta\lambda$) maps is significantly shifted from the plane defined by these three Fe atoms (Figure 3B and C). In addition, a 4-fold averaged $mF_{obs} - F_{calc}$ map calculated for crystal 2 shows a peak maximum at the expected position of the fourth metal in a regular [4Fe-4S] cluster. There is also significant electron density for a thiolate ligand at position 242 of the small subunit. These density features disappear when an iron ion and a thiolate are included in the model and a new $mF_{obs}-F_{calc}$ map is calculated with the resulting phases (Figure 3C). Finally, the high electron density observed in the ($\Delta\lambda$) map of the variant unambiguously shows that the fourth metal atom can only be Fe (Figure 3C).

All enzymes were isolated from the membrane fraction of the appropriate *E. coli* strain, indicating correct translocation to the membrane via the twin arginine translocation (Tat) system which would not translocate apoenzyme or incorrectly folded protein. Additionally, P242C and C19G/C120G/P242C are capable of H_2 oxidation in solution assays with rates that are, respectively, ∼50 and ∼10% of that observed with the native enzyme.[35]

Electrocatalysis of Variants. Electrocatalytic cyclic voltammograms (CVs) were measured over a potential range of −0.65 to +0.24 V at a scan rate of 5 mV s^{-1} (Figure 4). The H_2 atmosphere in the headspace was varied between 0.3−100% as indicated. Each enzyme shows negligible H_2 production activity at −0.65 V, even at lowest H_2 levels, as observed previously for native Hyd-1 under similar conditions.[8] The onset potential for H_2 oxidation activity is not affected in the variants compared to the native enzyme[8] and is the same regardless of H_2 concentration. (Conversely, the O_2-sensitive MBH Hyd-2 has minimal overpotential requirement for either hydrogen oxidation or proton reduction[8] and behaves as a reversible electrocatalyst.[54]) Measurements of K_m for H_2 gave similar values for all three enzymes (Figure S1A, Supporting Information). The CV experiments for each enzyme differ slightly in shape, with the native enzyme (>P242C > C19G/C120G/P242C) showing the most steeply climbing current before starting to level off, indicative of more efficient long-range electrocatalytic electron transfer (see also Figure S1B, Supporting Information). On the basis of the favorable comparisons among the three enzymes in terms of their electrocatalytic activity, we next tested the general model for O_2-tolerance during H_2 oxidation in terms of (1) the ability to avoid generation of Unready states during extended exposure to O_2, and (2) the ability to reactivate Ni−B rapidly (see also Figure 1).

Principles of Sustained H_2 Oxidation in the Presence of O_2: (1) Ensuring Formation of Ni−B Exclusively. *Differing Response to Transient and Prolonged Exposure to O_2.* To compare, directly, P242C and C19G/C120G/P242C with variants altered at the proximal cluster only, the same sets of experiments to gauge O_2-tolerance were performed as previously described.[9] The response to a short burst of concentrated O_2 (0.16 mM O_2 at 30 °C) was examined by cyclic voltammetry (Figure 5A), and chronoamperometry was used to monitor H_2 oxidation activity during prolonged exposure to O_2 (Figure 5B and C).

Response to Transient O_2 Exposure. Oxygen-saturated buffer was injected into the electrochemical cell at +0.03 V during the sweep to high potential of a slow CV scan (0.5 mV s^{-1}, from −0.43 → +0.24 → −0.43 V, 100% H_2) (Figure 5A). At the injection potential there is minimal reduction of O_2 at the surface of the electrode[8] and negligible anaerobic inactivation since the injection is performed at a potential

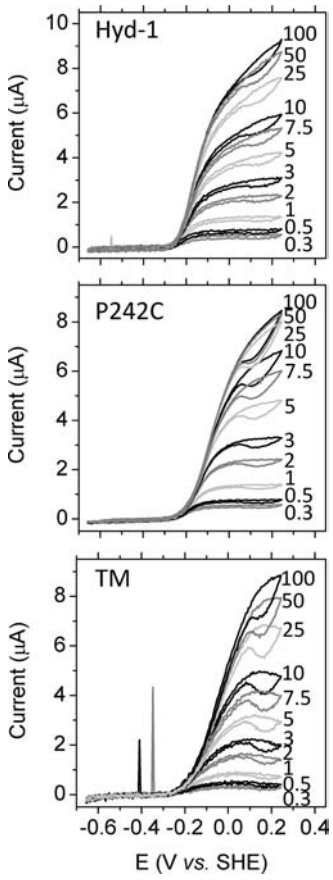

Figure 4. Catalytic response to H_2 at pH 6.0, 30 °C. Cyclic voltammograms were performed under different percentages of H_2 as indicated (right) for native Hyd-1, P242C and C19G/C120G/P242C (denoted TM). Ar was the carrier gas at a total gas flow rate of 1000 standard cubic centimeters (scc) min^{-1}. The potential was increased from −0.65 to +0.24 V and then reversed at 5 mV s^{-1}. Gas equilibration was monitored at 0 V prior to each scan (not shown), ω = 4500 rpm was used to avoid mass transport limitation at low hydrogen concentrations. Every 4th scan was performed under 100% H_2 to monitor film loss[56,57] (not shown). See Figure S1, Supporting Information, for Hanes analysis and determination of K_m and an overlay of the normalized cyclic voltammograms for each enzyme at 100% H_2.

well below E_{switch}[55] (+0.170 ± 0.01 V for all three enzymes at a scan rate of 0.5 mV s^{-1}, 100% H_2, data not shown). In all cases the current drops immediately upon addition of O_2, taking no more than a few seconds to reach a minimum value. The constant flow of 100% H_2 through the cell ensures that all O_2 injected is flushed out of the cell by the time the scan direction is reversed. The low K_m values for each enzyme (Figure S1, Supporting Information) ensure that the immediate response to the addition of O_2 is not complicated by the dilution of H_2.

The response to a transient burst of O_2 is assessed in two ways (denoted as *1 and *2 in Figure 5A): first, the ability of the enzyme to recover immediately (*1) following addition of O_2 (i.e., following the rapid drop caused by O_2 injection, the current *increases* before O_2 removal is complete and the scan direction is reversed); second, the ability to reactivate aerobically generated states on the return scan at a potential below E_{switch} (i.e., comparing the current of the oxidative and reductive sweeps at −0.1 V, Figure 5A, gray horizontal bars, *2). The only enzyme that satisfies condition *1 is native Hyd-1. Both the P242C and C19G/C120G/P242C continually inactivate as O_2 is flushed out. When the scan is reversed, activity rises in both native Hyd-1 and P242C. For C19G/C120G/P242C, however, almost all activity is abolished by the time the scan is reversed, and very little recovery is apparent on the return sweep to more negative potentials. The depth of the horizontal gray bar (*2 in Figure 5A), reflects the extent of formation of states that reactivate too slowly to have recovered by the time a potential of −0.1 V is reached. There is negligible formation of slowly recoverable states in native Hyd-1, as previously described,[9] but increased formation is apparent in both variants.

H_2 Oxidation Activity during Prolonged O_2 Exposure. Injections of O_2 give no information on how the active site responds to repeated attacks by O_2 over a longer time scale, so the ability to maintain substantial H_2 oxidation activity during prolonged O_2 exposure was examined (Figure 5B and C). Oxygen was introduced under a constant gas flow of 10% H_2 (with Ar as the carrier gas) at 0 V (i.e., well below E_{switch}) for all three enzymes (Figure 5B). In all cases the H_2 oxidation current drops as soon as O_2 is introduced into the headspace, that is, well before gas exchange is complete. This observation is in line with the immediate drop in current observed in CV experiments following O_2 injection (red arrow Figure 5A). For native Hyd-1, the O_2 level was incrementally stepped from 1% to 10%: importantly, at each increasing O_2 step the current settles to a new lower steady value (apart from slow film loss[56,57] that occurs throughout the long experiments, with or without O_2 present). This observation is discussed further below and highlighted in Figure 5B (green). In contrast, P242C and C19G/C120G/P242C do not attain a steady value but instead show a continual decrease in H_2 oxidation current even at just 1% O_2; consequently, the O_2 level was not increased further. Loss of activity is much faster for C19G/C120G/P242C (activity is almost negligible after ∼30 min) than for P242C. Figure 5C shows a similar experiment carried out with P242C but at the lower potential of −0.1 V, from which it is clear that activity loss is slower than at 0 V, yet nonetheless the current decreases continually and does not settle at a steady value.

The fact that the catalytic H_2 oxidation current for native Hyd-1 adjusts to a new steady-state level at each O_2 increment, rather than dropping continuously to zero, is crucial: it shows that at each step there must be a balance between the rate at which O_2 attacks and the rate that the enzyme recovers to resume catalysis. The steady-state condition requires that the fraction f of enzyme in the active state (fraction of current compared to that initially observed without O_2) is given by:

$$f = \frac{\text{rate of reactivation}}{\text{rate of reactivation} + \text{rate of inactivation}}$$

In order to assess the rates at which O_2 attacks, the initial rates of current decrease upon rapid injection of different amounts of O_2-saturated buffer were measured under the same conditions as used for the experiments in Figure 5B. Oxygen-saturated buffer was injected in the presence of 10% H_2 (0 V, 30 °C) simultaneously with the change in the O_2 concentration in the head space (Figure S2, Supporting Information) and the initial slope was measured for each O_2 concentration. The plot of initial rate against O_2 concentration was linear. The initial rate experiments were only carried out for native Hyd-1 since this is the only enzyme that sustains steady-state activity in the presence of O_2. Control experiments in which comparable

dx.doi.org/10.1021/ja311055d | J. Am. Chem. Soc. 2013, 135, 2694−2707

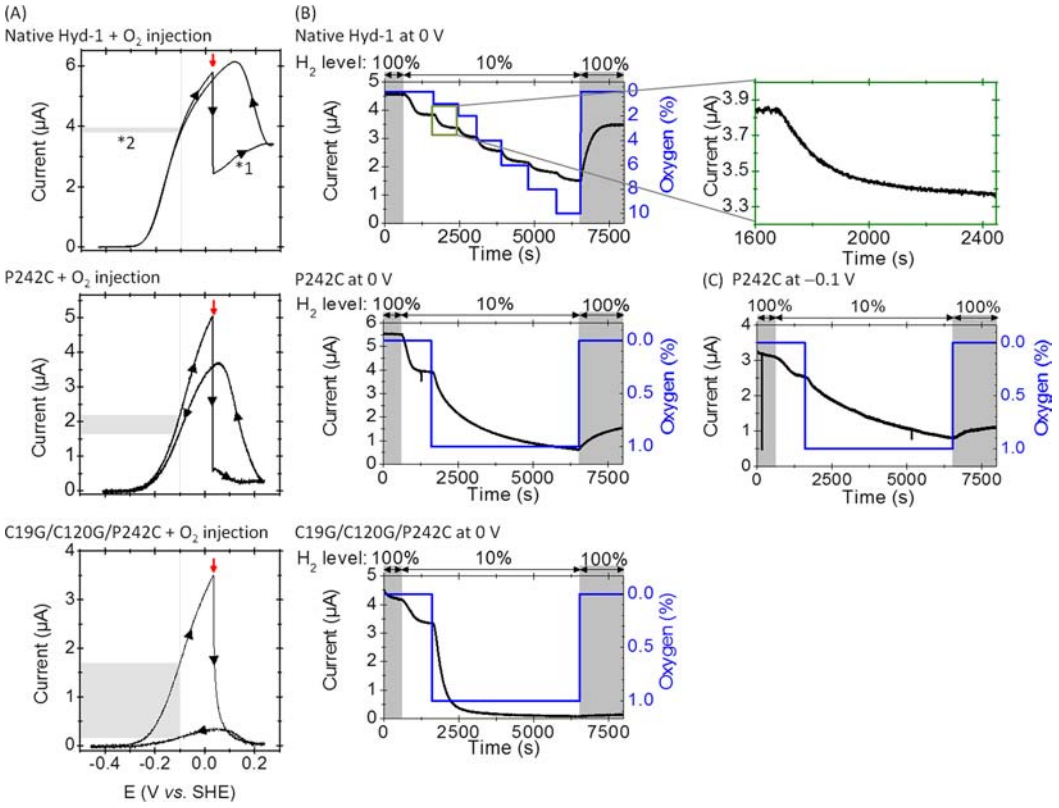

Figure 5. Effects on H_2 oxidation of transient (A) or prolonged (B and C) O_2 exposure: the latter experiments show that the variants undergo continual decline in activity even at 1% O_2 whereas native Hyd-1 adapts reversibly to each change up to at least 10% O_2. Cyclic voltammograms (A) were performed under a constant headgas atmosphere of 100% H_2. The potential was scanned between −0.41 and +0.24 V at 0.5 mV s^{-1}. At +0.03 V on the sweep to high potential, O_2-saturated buffer was injected to give a final O_2 concentration of 0.16 mM (indicated by a red arrow). By the point of scan reversal all O_2 had been flushed from the system. The depth of the gray horizontal bars indicates the difference in current of the forward and reverse scans at −0.1 V. Labels *1 and *2 indicate the characteristics used to assess the response to the transient burst of O_2 (see text for more details). Chronoamperograms (B and C) show current response (black) to various concentrations of O_2 (blue) at 0 V for all three enzymes (B) and at −0.1 V for P242C only (C). Initial current was measured at 100% H_2 for 600 s, then the H_2 level was lowered to 10%, and after 1000 s O_2 was introduced to the cell headspace. Initially, for all three enzymes, 1% O_2 was introduced, and in the case of native enzyme the O_2 content was increased stepwise to 10% as indicated. After a total O_2 exposure time of 5000 s, the headgas was returned to 100% H_2 and the final current monitored. The current response to 1% O_2 (i.e., the equivalent O_2 concentration used for each variant) is highlighted for native Hyd-1 (green box, B). All experiments were performed at pH 6.0 and 30 °C, ω = 3000 rpm, total gas flow rate = 1000 scc min^{-1}.

aliquots of Ar-saturated buffer were injected showed only very small, transient attenuations of current.

Upon returning to 100% H_2, native Hyd-1 reactivates within approximately 10 min, i.e. on the same time scale as O_2 is flushed from the system. The activity recovered is lower (approximately 80%) than measured at the start of the experiment but is accountable to slow film loss[56,57] over more than 2 h at 30 °C. This recovery is referred to as spontaneous because it occurs without lowering the electrode potential. In contrast, P242C exhibits spontaneous recovery to a much lesser extent, and C19G/C120G/P242C barely recovers at all.

Tolerance to CO. Carbon monoxide is a known competitive and reversible inhibitor of [NiFe]-hydrogenases, often used as a probe of gas access to and binding at the active site,[8,9] although the basis for the relationship between O_2 and CO tolerance is not clear. The O_2-tolerant enzymes show reduced sensitivity to inhibition by CO relative to O_2-sensitive enzymes.[8,58] Experiments (Figure S3, Supporting Information) showed that P242C and C19G/C120G/P242C are both capable of sustained H_2 oxidation in the presence of 20% CO and are therefore unchanged in this respect relative to native Hyd-1. All enzymes are thus classed as CO-tolerant when compared with Hyd-2 from *E. coli*.[8,9]

The above experiments reveal that the presence of a [3Fe-4S] cluster in the medial position is important for conferring O_2 tolerance. We therefore carried out experiments to assess the ability of P242C to form Ni−B rather than Unready states (including Ni−A). We have already reported that the proximal variants C19G and C19G/C120G are unable to avoid forming Unready states upon O_2 exposure,[9] so our PFE measurements focused on the P242C variant alone.

Response to Prolonged Anaerobic and Aerobic Inactivation. Anaerobically and aerobically generated inactive states were produced for both the native and P242C variant enzymes and are compared using CV experiments in Figure 6. Values of the potential at which rapid reductive reactivation is seen following anaerobic inactivation (E_{switch}[55]) were obtained by inactivating at high potential (+0.39 V) for 10000 s under 100% H_2 (Figure S4A, Supporting Information) and then scanning the electrode potential very slowly (0.1 mV s^{-1}) in the negative direction to drive reactivation (Figure 6A, red traces). This half cycle was immediately followed by a complete cycle (−0.6 → +0.39 → −0.6 V) (Figure 6A, black traces). For aerobic inhibition (Figure S4B, Supporting Information), the electrode

dx.doi.org/10.1021/ja311055d | J. Am. Chem. Soc. 2013, 135, 2694−2707

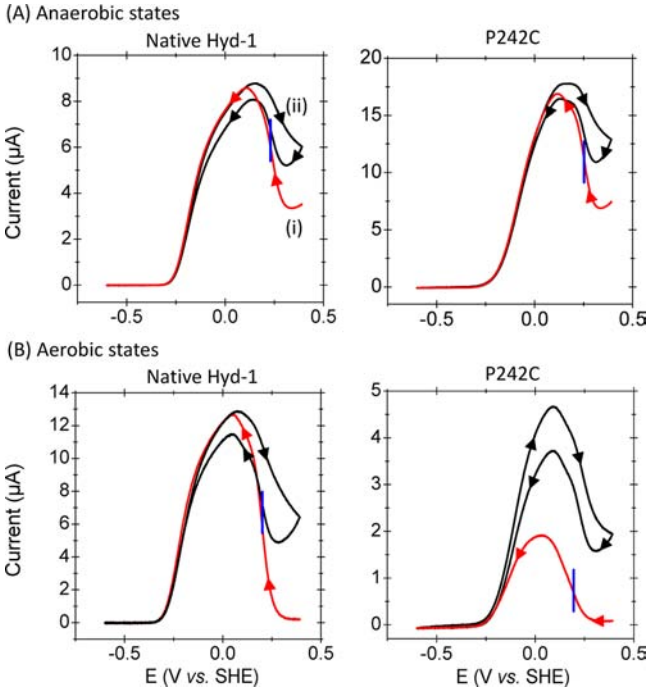

Figure 6. Cyclic voltammograms following anaerobic (A) and aerobic inactivation (B) for native Hyd-1 (left) and P242C (right). Following anaerobic or aerobic inhibition (see Figure S4 for details, Supporting Information), the potential was swept from +0.39 to −0.6 V (red, (i)). The scan direction was reversed immediately and the potential was swept back to +0.39 V followed by one final sweep to low potential (black, (ii)). Scan direction is indicated by arrow heads. The E_{switch}[55] values for the reactivation process on the first sweep to low potential (red) are indicated by vertical blue bars. All scans were conducted at 0.1 mVs^{-1}, pH 6.0, 30 °C, ω = 3000 rpm, 100% H_2, total gas flow rate = 1000 scc min^{-1}.

potential was first set at 0 V: the initial current under 100% H_2 was recorded, then the cell solution was equilibrated for 1000 s with 10% O_2 and 10% H_2 in Ar. Holding the potential at 0 V prevented anaerobic inactivation that occurs at higher potentials. The potential was then stepped to +0.39 V for 600 s to allow inactivation to occur. Oxygen was flushed from the cell for 1000 s before scanning to −0.6 V at 0.1 mV s^{-1} (Figure 6B, red traces) followed immediately by a complete cycle (−0.6 → +0.39 → −0.6 V) (Figure 6B, black traces). The initial scan (red) reveals the fraction of inactive states able to reactivate most rapidly whereas the subsequent, complete cycle (black) also reveals reactivated states that were not observed on the initial scan to low potential either because they require more negative potentials for reactivation (i.e., below the onset potential for H_2 oxidation) or could not reactivate in the time allowed.

As previously reported, native Hyd-1[9] shows no significant difference between anaerobically and aerobically generated states; reactivation occurs completely, at high potential, on the first sweep to negative potential (E_{switch} = +0.21 ± 0.02 V at a scan rate of 0.1 mV s^{-1}, blue vertical lines Figure 6A and B, left panels). Anaerobically generated states for P242C (E_{switch} = +0.22 ± 0.02 V at a scan rate of 0.1 mV s^{-1}, blue vertical line, Figure 6A, right) are also reactivated completely at high potential. Turning our attention to aerobically inactivated states, less than 50% of P242C is reactivated on the first sweep at a similar potential to that of native Hyd-1 (E_{switch} = +0.185 ± 0.02 V at a scan rate of 0.1 mV s^{-1}, blue vertical line, Figure 6B, right). The large increase in current in the subsequent cycle shows that much more P242C has been reactivated. Chronoamperometry (Figure S5, Supporting Information) reveals that unlike Hyd-1, which reactivates rapidly and completely at 0 V, a large fraction of P242C is only reactivated after a long period of time, with application of a more negative potential making little difference. Recovery of P242C following aerobic inactivation is multiphasic (Figure S6 and Figure S8, Supporting Information), showing at least two slow phases (differing in rate by an order of magnitude, Table S1, Supporting Information) in addition to the fast phase. Reactivation of the slow phases shows little potential dependence (Figure S7, Supporting Information).

Principles of Sustained H_2 Oxidation in the Presence of O_2: (2) Reactivation of Ni−B, Related Rates and Potentials. *Potential Dependence of the Rate of Reactivation of Ni−B.* Variants with the P242C mutation fail to attain a steady-state level of activity in the presence of O_2: instead, the catalytic current drops continuously to a very low level even in 1% O_2 (Figure 5B and C). To determine if a very much slower rate of reactivation of Ready state (Ni−B) is the cause of the increased O_2 sensitivity of P242C, the kinetics of reactivation were measured using chronoamperometry.[59] It was necessary to use low temperatures (5, 10, and 15 °C) to obtain the rate constants for reactivation of Ni−B because at higher temperatures the reaction was so fast that it was completely obscured by the initial charging current "spike" observed upon stepping the potential.[44] The enzymes were fully activated at −0.65 V for 600 s, then anaerobically inactivated at +0.39 V for 10000 s in 100% H_2 to form Ni−B/Ready. The potential was then stepped to a less positive value in the range +0.235 → +0.035 V, and the reactivation was monitored through the increase in current (see Figure S9 for examples, Supporting Information). The potential dependence of the rate of reactivation is shown in Figure 7. At potentials lower than +0.035 V, the rate of reactivation was too fast to measure accurately, even at 5 °C (not shown). Data were fitted using the two-step chronoamperometry model,[59] which takes into account the reversible reactivation of the Ready state at high potentials.

The current produced by active enzyme gives a direct indication of how the fraction of active enzyme changes with time:

$$[\text{Ready}] \underset{k_I}{\overset{k_A}{\rightleftharpoons}} [\text{active enzyme}]$$

where k_A describes the rate constant for reactivation of Ready, and k_I is the rate constant for inactivation back to the Ready form. The interconversion of these states through transient intermediates has been discussed[59] along with procedures for fitting data to the rate equation (see also Figure S9, Supporting Information).

The potential dependence of the rate of reactivation of Ni−B (k_A) at 5 °C (also at 10 and 15 °C, not shown) follows a linear free energy relationship (Figure 7 and see Supporting Information). There is no significant difference between native Hyd-1, the P242C or C19G/C120G variants (errors are well within an order of magnitude at +0.085 V) (Figure 7A). Viewed as a Tafel plot, the slopes of the plots of $\ln k_A$ versus potential ($-\alpha n F/RT$) give n = 1.1 in each case when fixing α at 0.5, that is, for a symmetrical electron-transfer process.[44] Additionally, the temperature dependence (at 5, 10, and 15 °C) of rate constants for native Hyd-1 and P242C follows the Arrhenius

dx.doi.org/10.1021/ja311055d | J. Am. Chem. Soc. 2013, 135, 2694−2707

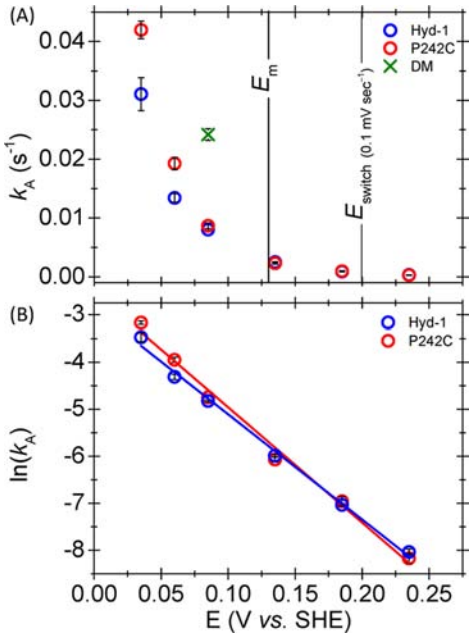

Figure 7. Rates of reductive reactivation (k_A) of the Ready states of native Hyd-1 (blue) and P242C (red) following a potential step (A, and see also Figure S9, Supporting Information), and the linear free energy relationship with potential (B). The rate of reactivation of Ni−B in the case of C19G/C120G (denoted DM) at +0.085 V is also included (green cross (A)). The midpoint potential (E_m) determined potentiometrically (Figure 8) for Ni−B along with E_{switch}[55] measured at 30 °C during a 0.1 mVs^{-1} CV scan,[62] (Figure 6) are shown as black vertical lines (A). Values for E_{switch} are scan-rate dependent as expected from the slow rates of activation at high potential, and the value shown is, within error, the same for C19G/C120G.[9] Inactivation (Figure S9, Supporting Information) was first induced by poising the electrode potential at +0.39 V for 10,000 s. Reductive activation was then monitored following a step to a lower potential in the range +0.235 to +0.035 V (see Supporting Information for details on fitting of data and Figure S9). Prior to each inactivation step, the electrode was poised at −0.65 V for 600 s to ensure enzyme was fully active. All experiments were performed at pH 6.0, 5 °C, 100% H_2 and total gas flow rate 100 scc min^{-1}, ω = 1000 rpm. Error bars are given as standard errors of the mean of three repeats. Due to the reversibility of the activation of Ni−B at high potentials, the potential dependence of the inactivation back to Ni−B (k_i) is given in Figure S10, Supporting Information.

relationship (Figure S11, Supporting Information) and data were fitted to the Arrhenius equation (see Supporting Information). These results allow us (with some assumptions) to estimate the rates of reactivation at more negative potentials and higher temperatures, both for the purpose of verifying the attainment of steady state at 30 °C and 0 V, and for assessing the functional implications under more physiological conditions.

An EPR-based titration was carried out to establish the midpoint potential at which Ni−B/Ready enzyme (a Ni^{III} species, $S = {}^1/_2$) is reduced to Ni^{II}. Potentiometric titrations of native Hyd-1 and P242C are complicated due to interactions of Ni(III) with the superoxidized proximal [4Fe-3S]$^{5+}$ cluster wherein the resulting enhanced relaxation leads to misleading intensities of the Ni signals.[35] We therefore used Hyd-1 variants in which the proximal cluster is EPR silent at high potentials (C19G/C120G and C19G/C120G/P242C).[9,35] Figure 8A compares X-band continuous-wave EPR spectra of "as-isolated"[52] samples of the C19G/C120G and C19G/C120G/P242C variants poised at selected potentials (full titrations are

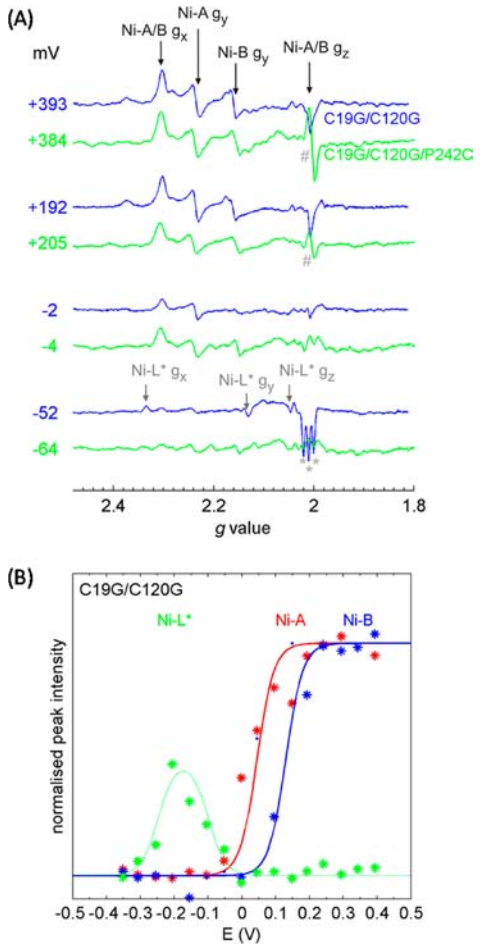

Figure 8. X-band CW EPR spectra of Hyd-1 variants C19G/C120G and C19G/C120G/P242C (A) and potentiometric titration of the Ni species in C19G/C120G illustrating the high midpoint potential of Ni−B (B). (A) Annotations (left) refer to the potential at which the samples were taken in mV (see Figure S12 for full titrations, Supporting Information). Measurement conditions: micro-wave frequency 9.384 GHz (C19G/C120G), 9.375 GHz (C19G/C120G/P242C); mw power 8 mV (C19G/C120G), 2 mV (C19G/C120G/P242C), modulation amplitude 1.0 mT (C19G/C120G), 1.4 mT (C19G/C120G/P242C); temperature 70 K (C19G/C120G), 80 K (C19G/C120G/P242C). "As-isolated" enzyme samples were used.[52] Enzyme concentrations: 21 μM (C19G/C120G), 22 μM (C19G/C120G/P242C). The g values for Ni−A/Ni−B and Ni−L* are indicated with arrows. Unidentified peaks are marked with an asterisk; these may be due to a nitroxide radical or trace amounts of free Fe^{3+} coordinated to a ^{14}N nucleus, as noted previously,[9,35] and have also been observed in preparations from other O_2-tolerant hydrogenases.[74−76] Peaks arising from mediators (phenazine methosulfate) are marked with #. (B) Peak intensities of the EPR active species in the C19G/C120G variant as a function of potential, computed using g_y for Ni−A/Ni−B and g_x for Ni−L*, and fitted (by eye) to one-electron Nernst equations with midpoint potentials E_m (Ni−A) = +45 ± 30 mV, E_m (Ni−B) = +130 ± 20 mV, $E_{m(app)}$ (Ni−L*) = −100 ± 20 and −247 ± 20 mV. The "midpoint" potentials for Ni−L* are apparent (app) values for the "appearance" and "disappearance" of this state; in the absence of the EPR-silent Ni−SI and Ni−R species the "true" midpoint potentials cannot be determined. The calculated "Nernst plot" for Ni−L* is therefore shown as a dotted line and the maximum intensity scaling of the highest intensity Ni−L* peak is arbitrary. The peak intensities depicted as • in the Ni−B Nernst plot result from samples following reduction and anaerobic reoxidation, in which a consistent shift in the Ni−B g_y values was observed (Figure S12, Supporting Information).

dx.doi.org/10.1021/ja311055d | J. Am. Chem. Soc. 2013, 135, 2694−2707

provided in Figure S12, Supporting Information) using temperatures at which the rapidly relaxing Fe−S cluster spins are not observed. As reported previously[35] (and discussed later) the medial $[4Fe\text{-}4S]^{+}$ cluster of P242C and C19G/C120G/P242C is not revealed by EPR. The peak intensities of the EPR-active Ni species in C19G/C120G as a function of potential follow the Nernst equation for a one-electron process (Figure 8B). Because the g_x (2.31) and g_z (2.01) peaks of Ni−A and Ni−B overlap, only the g_y peaks could be used to extract midpoint potentials.[60] The midpoint potential for the disappearance of Ni−B is +130 ± 20 mV and that of Ni−A is +45 ± 30 mV (Table S4, Supporting Information). The Ni−L* species, which has g values and coupling patterns to the reduced proximal cluster similar to those generally associated with Ni−L,[35,61] is apparent at moderately low potentials (with maximum intensity around −185 mV) and disappears at more negative potentials as the EPR-silent Ni−R species is/are formed. We previously reported[35] that Hyd-1 and variants do not exhibit Ni−C signals and the presence of Ni−L*—which appears without illumination—is currently under investigation. As previously noted,[9] the Ni−B g_y peak shifts slightly (from 2.16 to 2.17) following reduction and anaerobic reoxidation (represented as blue • in Figure 8B). Although insufficient data points were available to obtain an accurate midpoint potential for reoxidation, it appears that the potential of this "recycled" Ni−B is less positive than that of "as-isolated" Ni−B and more comparable to that of Ni−A (see Figure 8B). In contrast, the spectrum and midpoint potential for Ni−A are unaffected upon anaerobic reoxidation. The data obtained for the C19G/C120G/P242C variant were not of sufficient intensity to obtain accurate Nernst plots, but Figure 8A clearly shows that Ni−A and Ni−B are fully reduced at −64 mV, indicating that their reduction potentials are comparable to those for C19G/C120G.

DISCUSSION

Previous studies have demonstrated the importance of the proximal cluster in conferring O_2-tolerance to a class of [NiFe]-hydrogenases. The special $[4Fe\text{-}3S]^{5+/4+/3+}$ cluster has the unique ability to deliver two electrons rapidly to the active site over a narrow potential range.[35,36] The results we have presented now demonstrate that substitution of just one amino acid at the medial [3Fe-4S] cluster is as lethal as the double exchange in C19G/C120G[9] and, once again, the effect is manifested through the inability to sustain any steady-state level of activity, even in 1% O_2. The crystallography confirms that in P242C the medial cluster is converted to a [4Fe-4S] cluster, which should have a more negative reduction potential.[44] The mechanistic role of the native [3Fe-4S] cluster has thus been examined, extending our understanding of the importance of the individual Fe−S clusters further down the electron relay.

Shape of the O_2 Inactivation Traces. All the enzymes react rapidly with O_2 as evidenced by the immediate drop in activity when O_2-saturated buffer is injected during cyclic voltammetry (Figure 5A). However, in these experiments, O_2 immediately begins to be flushed from the system under the constant flow of H_2 through the head space. Chronoamperometry in the prolonged presence of O_2 (Figure 5B and C) is more informative and reveals striking differences between the native enzyme and the two variants. Under 10% H_2, Hyd-1 sustains a significant current as O_2 is sequentially stepped from 1% to 10%; importantly, at each increase in O_2 partial pressure the H_2 oxidation current of Hyd-1 settles to a new steady level. When the same experiment is carried out for the native enzyme at a lower potential (−0.1 V) the drops in current at each O_2 step are much smaller.[9] When the gas atmosphere is returned to 100% H_2, all expected current is restored. In contrast, P242C undergoes continual inactivation in just 1% O_2 at both 0 and −0.1 V, as does C19G/C120G/P242C (for which the current falls more rapidly, even at 0 V) so a steady-state fraction of active enzyme is never achieved. For P242C, restoring the atmosphere to 100% H_2 produces only a very limited increase in current, and the same gas change for C19G/C120G/P242C barely registers, thus demonstrating the formation of Unready states.

The observation that for native Hyd-1 H_2 oxidation activity in the presence of O_2 is simply attenuated to a new level for each O_2 concentration leads to the following conclusions: (a) that Hyd-1 avoids making Unready states, otherwise activity would continuously fall as seen in the variants; (b) at each new steady level the rate of activation of Hyd-1 must equal the rate of inactivation. A steady state is not achieved for the variants because reactivation of Unready states is so much slower than inactivation. The extreme sensitivity of C19G/C120G/P242C even to transient O_2 exposure is not surprising since Hyd-1 variants lacking a cysteine at position 19 coordinating the proximal cluster are already sensitive to a short burst of O_2.[9]

Accumulation of Unready States. The tolerance of P242C to O_2 increases as a more negative potential is imposed, as observed previously for the native enzyme, proximal cluster variants,[9] and *Re*-MBH.[11] Despite the higher rate of reactivation of Ni−B at more negative potentials (Figure 7), steady-state H_2 oxidation activity is never sustained for P242C, and this must be due to formation of Unready states. Reactivation of those Unready states is slow and not greatly enhanced at lower potential (Figure S7, Supporting Information). The net result is that formation of Unready states of P242C is essentially irreversible, and continuous reactivation of Ni−B/Ready in the constant presence of O_2/H_2 results in accumulation of those Unready states (Figure S8, Supporting Information). The variants are eventually overwhelmed by O_2. These accumulated states are only capable of reactivation over greatly *extended* time periods when O_2 is removed and H_2 is provided (Figure S5 and Figure S8, Supporting Information) and their reactivation is not significantly enhanced at more negative potentials (Figure S7, Supporting Information). The slow reactivation of P242C Unready states regardless of potential is different to that seen with proximal cluster variants of Hyd-1 where Unready states are activated only at a much lower potential,[9] suggesting that the Unready states formed by P242C differ from those formed by proximal cluster variants.

Reactivation. The rate constant (k_A) for reactivation of the Ready state is not significantly affected by point mutations at the medial and/or proximal clusters: the potential dependence of k_A is exponential for both the native and variant P242C enzymes and, moreover, C19G/C120G shows a similar k_A at +0.085 V (Figure 7) despite also being O_2 sensitive.[9] The inability of the variants to maintain H_2 oxidation activity in the presence of O_2 is therefore not caused by a change in the rate of reactivation of Ni−B/Ready. Converting the medial [3Fe-4S] cluster into a [4Fe-4S] cluster removes the ability of the enzyme to avoid accumulating Unready states under O_2: in this respect the medial cluster is as important as the proximal cluster.

dx.doi.org/10.1021/ja311055d | J. Am. Chem. Soc. 2013, 135, 2694−2707

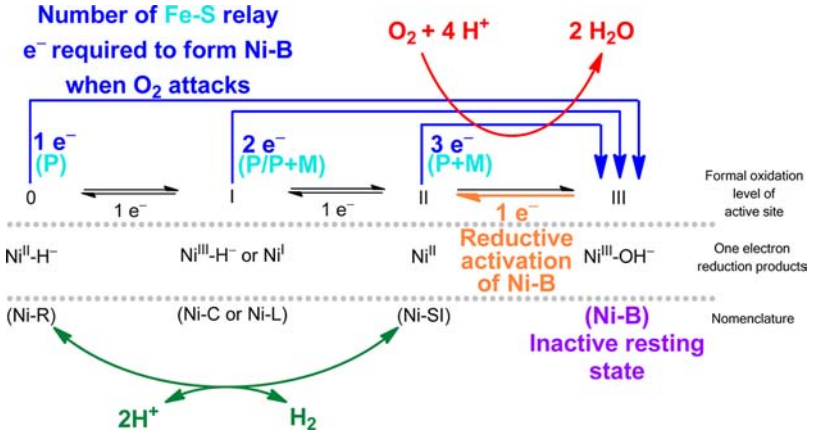

Figure 9. Hydrogen-oxidase catalytic cycle of Hyd-1 summarizing the results and conclusions of this work. The hydrogenase cycle is shown in green. The number of electrons (blue) required from the Fe−S relay to form Ni−B (purple) upon O_2 attack (red) is shown. Completion of the oxidase cycle by complete four electron reduction of O_2 requires reduction of Ni−B and is shown in orange. The Fe−S clusters are denoted as P (proximal) and M (medial). The Fe−S cluster(s) involved in electron discharge to the active site are shown in cyan.

The rate of reactivation of Ni−B increases exponentially with decreasing potential and is slow at values corresponding to E_{switch}[62] (Figure 7). There is no general agreement as to the basis of E_{switch}—whether it should be interpreted in a thermodynamic sense, that is, a high value of E_{switch} correlates with a low redox stability of Ni−B or whether it relates more to the kinetics of reactivation of Ni−B. The reduction potentials for Ni−A and Ni−B in various O_2-tolerant and O_2-sensitive [NiFe]-hydrogenases determined by EPR or FTIR are compared in Table S4, Supporting Information. The PFE and titration experiments necessarily differ because H_2 (which must stabilize active states) is nearly always present or absent respectively. Our EPR titrations show, unequivocally, that Ni−B is reduced at relatively high potentials (Table S4, Figures 8 and S12, Supporting Information) for the variants altered at the medial and/or proximal clusters in Hyd-1 and most certainly also for native Hyd-1 and P242C although these values could not be determined directly by EPR, as mentioned previously.[35,61] Specifically, the midpoint potential for C19G/C120G is approximately +130 mV at pH 6.0 and 20 °C, and E_{switch} for the same variant is approximately +200 mV at pH 6.0 albeit at 30 °C when measured at the slowest scan rate of 0.1 mVs^{-1}.[62]

We therefore conclude that the mutations at the medial or proximal cluster do not significantly affect the rate *or* potential of reactivation of Ni−B (see (2) in Figure 1), but instead destroy the ability to form *only* Ni−B upon reaction with O_2 (see (1) in Figure 1).

Extrapolation of the linear free energy (Figure 7B) and Arrhenius plots (Figure S11, Supporting Information) allows us to estimate k_A at a given potential and temperature, assuming there is no change in the rate-limiting step with potential or temperature. In line with the model for O_2 tolerance (Figure 1) the fact that Ni−B in Hyd-1 is reactivated at potentials >+100 mV means that even at more oxidizing potentials, reduction of Ni−B to active enzyme will still be spontaneous. Viewed in terms of the familiar Tafel plot, the log-slope of the exponential potential dependence provides compelling evidence that reactivation of Ni−B is a one-electron process, in other words Ni(III) is reduced to Ni(II). At 37 °C and −0.1 or 0 V, similar rates of reactivation of Ni−B for P242C and native Hyd-1 are predicted by extrapolation (~2.9 s^{-1} and ~1.5 s^{-1} at −0.1 V respectively and ~0.25 s^{-1} at 0 V for both enzymes). Using a value of 0.20 s^{-1} estimated for native Hyd-1 at 30 °C and 0 V gives good agreement (within 20%) with the steady-state currents shown in Figure 5B (f_{obs}/f_{calc} values (at each $\%O_2$) are 1%: 0.83/0.90; 2%: 0.71/0.82; 4%: 0.56/0.68; 6%: 0.45/0.55; 8%: 0.38/0.45; 10%: 0.33/0.39).

Reactivation of Ni−B completes a catalytic cycle, with a low but significant rate that raises the interesting possibility that native Hyd-1 could act as a reasonably competent oxygen reductase (Figure 9) under physiological conditions, in addition to being a H_2-quinone oxidoreductase.[63] The crystal structure of native Hyd-1[34] shows it to be a dimer $(SL)_2$ of heterodimers (SL), which could exist under physiological conditions. A special significance of this quaternary structure is indicated by the close proximity of the distal clusters of each SL heterodimer, so that electrons required by the active site under O_2 attack on one SL heterodimer can be provided by rapid H_2 oxidation at the active site of the connected SL heterodimer.

The potential evolutionary significance of the observed oxygen reductase activity of *E. coli* Hyd-1 is intriguing. [NiFe]-hydrogenases are thought to be among the most ancient enzymes of biotic Earth,[3] even predating the *L*ast *U*niversal *C*ommon *A*ncestor (LUCA) before prokaryotic life split into the Bacterial and Archaeal domains.[64] The evolution of life on Earth proceeded for some 2×10^9 years, with anaerobic H_2 respiration thought to be a major energy source, before O_2 started to accumulate at significant concentrations due to oxygenic photosynthesis.[65] The transition from a reducing anoxic atmosphere to an oxidizing one was a very slow process and it has been estimated that O_2 levels rose from ~2 ppm 2.5 $\times 10^9$ years ago to 880 ppm 700 million years later.[65] The emergence of O_2, and associated reactive oxygen species, would have posed a problem to early prokaryotic cells—not least because O_2-sensitive respiratory [NiFe]-hydrogenases would have been irreversibly inactivated. Recent evolutionary analysis of the O_2-tolerant hydrogenases bearing the [4Fe-3S] proximal cluster suggests these enzymes might predate the emergence of O_2 and if so, were already present and active in prokaryotic populations as O_2 levels began to rise.[66] Given that highly specialized, copper-dependent oxygen reductases could only have evolved after the appearance of O_2 in the atmosphere,[64] it is tempting to speculate that the nickel-dependent progenitors of the O_2-tolerant hydrogenases could represent the first true

oxidases with the proven ability to perform a four-electron reduction of O_2 to harmless water, albeit at low rates.

As argued earlier, three relay-derived electrons are required to deal with O_2 attack at the active site in its most oxidized (electron-poor) active level (Ni−SI). The importance of the proximal cluster's ability to provide two electrons has already been demonstrated.[34−36] These electrons are discharged at high potential, which is not a problem in terms of thermodynamic reducing power because O_2 and all intermediates are strongly oxidizing anyway (except for the initial oxygen-to-superoxide one-electron reduction that has a quite negative potential[67]). The active site itself can always provide the first electron to reduce O_2 to superoxide. Importantly, centers having high reduction potentials, including the medial [3Fe-4S] cluster, are far more likely to have an electron bound and ready for immediate transfer back to the active site. We recently reported on the high reduction potential of the medial [3Fe-4S] cluster in the native enzyme, and noted that we could not observe the reduced $[4Fe\text{-}4S]^+$ medial cluster of P242C by EPR.[35] Experiments with super-reducing Europium complexes (Eu-DTPA) did not reveal any reduction of the converted [4Fe-4S] cluster and we concluded that its ground state is not $S = {}^1/_2$. On the basis of other evidence (see below), it is highly likely that the converted [4Fe-4S] medial cluster in P242C has a more negative reduction potential than the [3Fe-4S] cluster in Hyd-1 and will not so readily have an electron available. The medial [4Fe-4S] cluster of the [NiFeSe]-hydrogenase from *Dm. baculatum*[68] has a reduction potential of −315 ± 20 mV at pH 7.6.[69] Protein film electrochemistry studies demonstrated that the enzyme cannot oxidize H_2 in the presence of O_2 but is capable of H_2 production in the presence of low O_2 concentrations (1%).[70] Reactivation of the aerobically generated inactive state(s) does not occur until a potential of approximately −350 mV at pH 6.0 and as such oxygen tolerant H_2 oxidation is not exhibited.[70] There are several examples of 3Fe and 4Fe cluster interconversions through point mutation: a valine-to-cysteine variant in *E. coli* fumarate reductase resulted in a change in potential from −70 mV ($[3Fe\text{-}4S]^{1+/0}$) to −350 mV ($[4Fe\text{-}4S]^{2+/1+}$).[71] Importantly, a [3Fe-4S] to [4Fe-4S] cluster conversion in the standard hydrogenase P238C variant from *D. fructosovorans* was reported to be accompanied by a decrease in potential from +65 to −250 mV.[38] Bingemann et al. made the reverse mutation, C205P, in the small subunit of the F420-reducing [NiFeSe]-hydrogenase from *Methanococcus voltae*, and the midpoint potential of the resulting [3Fe-4S] cluster was more than 400 mV more positive than that of the native [4Fe-4S] cluster.[72]

Through PFE we are able to control the potential directly and thus influence the predominant oxidation level of the active site and the number of electrons available at the time of O_2 attack (Figure 1). Comparing the response of P242C to O_2 at 0 and −0.1 V (Figure 5B and C) demonstrates that O_2-tolerance is increased, albeit in a limited way, by favoring more reduced states at active site. If, for instance, attack by O_2 occurs at the Ni−C level, all four electrons required for its complete reduction can be supplied by the bridging hydride (2 e^-) and the proximal cluster (2 e^-), leading to Ni−B.

CONCLUSIONS

The basis of O_2-tolerance in Hyd-1, and most likely other membrane-bound [NiFe]-hydrogenases, is that all the electrons required to reduce O_2 to water are readily available within the enzyme and immediately transferable to the active site when required. The role of the medial cluster becomes critical when O_2 attacks the more oxidized active Ni−SI state in which case only one electron can be immediately supplied by the oxidation of Ni^{II} to Ni^{III}. This situation may prevail under conditions of high potentials and/or low H_2 levels. Although two more electrons are provided by the proximal cluster, a subject of very recent studies,[34−36] the crucial *fourth* electron (or third electron from the Fe−S relay) must be obtained from the high potential[35] medial cluster. We depict this conclusion in Figure 9 in terms of the importance of Ni−B formation (see also (1) in Figure 1) and its rapid reactivation (see also (2) in Figure 1). Starting at the most oxidized active state of the [NiFe] site (Ni−SI), with each successive formal reduction of the active site Ni prior to O_2 attack, one less Fe−S relay electron (blue) is required to ensure Ni−B formation (purple), and therefore an electron from the medial cluster becomes less vital in the immediate neutralization of attacking O_2. In the worst case scenario, when O_2 attacks at the level of Ni−SI, the medial cluster is essential: Ni−B (a Ni(III)−OH species), the product of four-electron reduction of O_2, represents a safe haven against further O_2 attack; hence, fast delivery of these three electrons (the maximum required) is critical. Re-entry into the catalytic cycle from Ni−B requires reduction of the active site Ni from Ni^{III} to Ni^{II} and release of the OH^- (H_2O). This last step results in active hydrogenase and closes the "oxidase cycle", the four electron reduction of O_2 (orange). Given the guaranteed availability (within the active site and relay) of all of the electrons required to form Ni−B and avoid partially reduced oxygen species, it follows that rapid reduction of Ni−B (Ni^{III}) at physiological potentials then allows significant and sustained (steady state) H_2 oxidation activity in the presence of O_2.

ASSOCIATED CONTENT

Supporting Information

Supporting Figures and Tables detail the determination of K_m for H_2, examining the rate of reaction with O_2 and tolerance to CO, inhibition procedures for generation of anaerobically and aerobically inactivated states, rates of formation and of reactivation of inhibited states, and potentiometric EPR titrations of Hyd-1 enzymes. This material is available free of charge via the Internet at http://pubs.acs.org.

AUTHOR INFORMATION

Corresponding Author

fraser.armstrong@chem.ox.ac.uk

Notes

The authors declare no competing financial interest.

ACKNOWLEDGMENTS

This research was supported by the Engineering and Physical Sciences Research Council (Grant EP/D044855D/1, supporting the Oxford Centre for Advanced Electron Spin Resonance, CAESR), by the Biological and Biotechnological Sciences Research Council (Grants BB/H003878-1 and BB/I022309-1) and previous grants from the Agence Nationale de la Recherche Scientifique. We thank Elena Nomerotskaia for help with protein purification.

REFERENCES

(1) Jones, A. K.; Sillery, E.; Albracht, S. P. J.; Armstrong, F. A. *Chem. Commun.* **2002**, 866−867.

(2) Hambourger, M.; Gervaldo, M.; Svedruzic, D.; King, P. W.; Gust, D.; Ghirardi, M.; Moore, A. L.; Moore, T. A. *J. Am. Chem. Soc.* **2008**, *130*, 2015−2022.
(3) Vignais, P. M.; Billoud, B.; Meyer, J. *FEMS Microbiol. Rev.* **2001**, *25*, 455−501.
(4) Ballantine, S. P.; Boxer, D. H. *J. Bacteriol.* **1985**, *163*, 454−459.
(5) Sawers, R. G.; Boxer, D. H. *Eur. J. Biochem.* **1986**, *156*, 265−275.
(6) Ballantine, S. P.; Boxer, D. H. *Eur. J. Biochem.* **1986**, *156*, 277−284.
(7) Sawers, R. G.; Ballantine, S. P.; Boxer, D. H. *J. Bacteriol.* **1985**, *164*, 1324−1331.
(8) Lukey, M. J.; Parkin, A.; Roessler, M. M.; Murphy, B. J.; Harmer, J.; Palmer, T.; Sargent, F.; Armstrong, F. A. *J. Biol. Chem.* **2010**, *285*, 3928−3938.
(9) Lukey, M. J.; Roessler, M. M.; Parkin, A.; Evans, R. M.; Davies, R. A.; Lenz, O.; Friedrich, B.; Sargent, F.; Armstrong, F. A. *J. Am. Chem. Soc.* **2011**, *133*, 16881−16892.
(10) Hexter, S. V.; Grey, F.; Happe, T.; Climent, V.; Armstrong, F. A. *Proc. Natl. Acad. Sci. U.S.A.* **2012**, *109*, 11516−11521.
(11) Cracknell, J. A.; Wait, A. F.; Lenz, O.; Friedrich, B.; Armstrong, F. A. *Proc. Natl. Acad. Sci.* **2009**, *106*, 20681−20686.
(12) Friedrich, B.; Fritsch, J.; Lenz, O. *Curr. Opin. Biotechnol.* **2011**, *22*, 358−364.
(13) Montet, Y.; Amara, P.; Volbeda, A.; Vernede, X.; Hatchikian, E. C.; Field, M. J.; Frey, M.; Fontecilla-Camps, J. C. *Nat. Struct. Mol. Biol.* **1997**, *4*, 523−526.
(14) Volbeda, A.; Montet, Y.; Vernède, X.; Hatchikian, E. C.; Fontecilla-Camps, J. C. *Int. J. Hydrogen Energy* **2002**, *27*, 1449−1461.
(15) Buhrke, T.; Lenz, O.; Krauss, N.; Friedrich, B. *J. Biol. Chem.* **2005**, *280*, 23791−23796.
(16) Duché, O.; Elsen, S.; Cournac, L.; Colbeau, A. *FEBS J.* **2005**, *272*, 3899−3908.
(17) Dementin, S.; Leroux, F.; Cournac, L.; de Lacey, A. L.; Volbeda, A.; Léger, C.; Burlat, B.; Martinez, N.; Champ, S.; Martin, L.; Sanganas, O.; Haumann, M.; Fernández, V. c. M.; Guigliarelli, B.; Fontecilla-Camps, J. C.; Rousset, M. *J. Am. Chem. Soc.* **2009**, *131*, 10156−10164.
(18) Lamle, S. E.; Albracht, S. P. J.; Armstrong, F. A. *J. Am. Chem. Soc.* **2004**, *126*, 14899−14909.
(19) Volbeda, A.; Martin, L.; Cavazza, C.; Matho, M.; Faber, B. W.; Roseboom, W.; Albracht, S. P. J.; Garcin, E.; Rousset, M.; Fontecilla-Camps, J. C. *J. Biol. Inorg. Chem.* **2005**, *10*, 239−249.
(20) Fontecilla-Camps, J. C.; Volbeda, A.; Cavazza, C.; Nicolet, Y. *Chem. Rev.* **2007**, *107*, 4273−4303.
(21) Kumar, M.; Colpas, G. J.; Day, R. O.; Maroney, M. J. *J. Am. Chem. Soc.* **1989**, *111*, 8323−8325.
(22) Darensbourg, M. Y.; Weigand, W. *Eur. J. Inorg. Chem.* **2011**, *2011*, 994−1004.
(23) van Gastel, M.; Stein, M.; Brecht, M.; Schröder, O.; Lendzian, F.; Bittl, R.; Ogata, H.; Higuchi, Y.; Lubitz, W. *J. Biol. Inorg. Chem.* **2006**, *11*, 41−51.
(24) Asso, M.; Guigliarelli, B.; Yagi, T.; Bertrand, P. *Biochim. Biophys. Acta: Protein Struct. Mol. Enzymol.* **1992**, *1122*, 50−56.
(25) Fernandez, V. M.; Hatchikian, E. C.; Cammack, R. *Biochimica et Biophysica Acta: Protein Struct. Mol. Enzymol.* **1985**, *832*, 69−79.
(26) Jones, A. K.; Lamle, S. E.; Pershad, H. R.; Vincent, K. A.; Albracht, S. P. J.; Armstrong, F. A. *J. Am. Chem. Soc.* **2003**, *125*, 8505−8514.
(27) De Lacey, A. L.; Hatchikian, E. C.; Volbeda, A.; Frey, M.; Fontecilla-Camps, J. C.; Fernandez, V. M. *J. Am. Chem. Soc.* **1997**, *119*, 7181−7189.
(28) Mege, R. M.; Bourdillon, C. *J. Biol. Chem.* **1985**, *260*, 14701−14706.
(29) Fritsch, J.; Scheerer, P.; Frielingsdorf, S.; Kroschinsky, S.; Friedrich, B.; Lenz, O.; Spahn, C. M. T. *Nature* **2011**, *479*, 249−252.
(30) The exact structure of the Ni−R state(s) is uncertain. Indeed, there are many examples in the literature where Ni−R exists in more than one substate. [NiFe]-hydrogenases from different organisms have been investigated in terms of the potential dependence of the interconversion of these IR-detectable substates (see Fichtner et al. 2006 for discussion). Whatever the exact nature of Ni−R, it is still the three electron reduction product of Ni−B.
(31) Fichtner, C.; Laurich, C.; Bothe, E.; Lubitz, W. *Biochemistry* **2006**, *45*, 9706−9716.
(32) Goris, T.; Wait, A. F.; Saggu, M.; Fritsch, J.; Heidary, N.; Stein, M.; Zebger, I.; Lendzian, F.; Armstrong, F. A.; Friedrich, B.; Lenz, O. *Nat. Chem. Biol.* **2011**, *7*, 310−318.
(33) Shomura, Y.; Yoon, K.-S.; Nishihara, H.; Higuchi, Y. *Nature* **2011**, *479*, 253−256.
(34) Volbeda, A.; Amara, P.; Darnault, C.; Mouesca, J.-M.; Parkin, A.; Roessler, M. M.; Armstrong, F. A.; Fontecilla-Camps, J. C. *Proc. Natl. Acad. Sci.* **2012**, *109*, 5305−5310.
(35) Roessler, M. M.; Evans, R. M.; Davies, R. A.; Harmer, J.; Armstrong, F. A. *J. Am. Chem. Soc.* **2012**, *134*, 15581−15594.
(36) Pandelia, M.-E.; Nitschke, W.; Infossi, P.; Giudici-Orticoni, M.-T.; Bill, E.; Lubitz, W. *Proc. Natl. Acad. Sci.* **2011**, *108*, 6097−6102.
(37) Beinert, H.; Holm, R. H.; Münck, E. *Science* **1997**, *277*, 653−659.
(38) Rousset, M.; Montet, Y.; Guigliarelli, B.; Forget, N.; Asso, M.; Bertrand, P.; Fontecilla-Camps, J. C.; Hatchikian, E. C. *Proc. Natl. Acad. Sci. U.S.A.* **1998**, *95*, 11625−11630.
(39) Teixeira, M.; Moura, I.; Xavier, A. V.; Moura, J. J. G. *J. Biol. Chem.* **1989**, *264*, 16435−16450.
(40) Vincent, K. A.; Parkin, A.; Armstrong, F. A. *Chem. Rev.* **2007**, *107*, 4366−4413.
(41) Casadaban, M. J.; Cohen, S. N. *Proc. Natl. Acad. Sci.* **1979**, *76*, 4530−4533.
(42) Dubini, A.; Pye, R. L.; Jack, R. L.; Palmer, T.; Sargent, F. *Int. J. Hydrogen Energy* **2002**, *27*, 1413−1420.
(43) Sucheta, A.; Cammack, R.; Weiner, J.; Armstrong, F. A. *Biochemistry* **1993**, *32*, 5455−5465.
(44) Bard, A. J.; Faulkner, L. R. *Electrochemical methods*; Wiley: New York, 2001.
(45) Vernède, X.; Fontecilla-Camps, J. C. *J. Appl. Crystallogr.* **1999**, *32*, 505−509.
(46) Kabsch, W. *Acta Crystallogr., Sect. D* **2010**, *66*, 125−132.
(47) McCoy, A. J.; Grosse-Kunstleve, R. W.; Adams, P. D.; Winn, M. D.; Storoni, L. C.; Read, R. J. *J. Appl. Crystallogr.* **2007**, *40*, 658−674.
(48) Emsley, P.; Lohkamp, B.; Scott, W. G.; Cowtan, K. *Acta Crystallogr., Sect. D* **2010**, *66*, 486−501.
(49) Murshudov, G. N.; Skubak, P.; Lebedev, A. A.; Pannu, N. S.; Steiner, R. A.; Nicholls, R. A.; Winn, M. D.; Long, F.; Vagin, A. A. *Acta Crystallogr., Sect. D* **2011**, *67*, 355−367.
(50) Winn, M. D.; Ballard, C. C.; Cowtan, K. D.; Dodson, E. J.; Emsley, P.; Evans, P. R.; Keegan, R. M.; Krissinel, E. B.; Leslie, A. G. W.; McCoy, A.; McNicholas, S. J.; Murshudov, G. N.; Pannu, N. S.; Potterton, E. A.; Powell, H. R.; Read, R. J.; Vagin, A.; Wilson, K. S. *Acta Crystallogr., Sect. D* **2011**, *67*, 235−242.
(51) Read, R. J. *Acta Cryst. A* **1986**, *42*, 140−149.
(52) The term "as-isolated" refers to Hyd-1 that has not been grown and purified under H_2 and is typically found in a mixture of Ni−A, Ni−B, and other Unready states (Lukey et al., 2010 and 2011).
(53) Bradford, M. M. *Anal. Biochem.* **1976**, *72*, 248−254.
(54) Armstrong, F. A.; Hirst, J. *Proc. Natl. Acad. Sci.* **2011**, *108*, 14049−14054.
(55) We use the term E_{switch} here as the potential given by the minimum of the first derivative (di/dE) of the reductive sweep of a CV scan (Vincent et al., 2007). E_{switch} is known to depend on many experimental parameters such as scan rate, extent of inactivation to Ni−B prior to the reductive sweep, temperature and pH. Whatever the exact origin of E_{switch} is it serves as a very useful guide as to the ease of reactivation of Ni−B when the experimental conditions used are identical for each enzyme.
(56) Film loss describes the exponential and irreversible loss of current over time as enzyme unfolds and/or desorbs from the electrode surface. The level of film loss is dependent on a number of factors such as the conditions of the experiment and the potential the electrode is poised at. It can also be dependent upon the way in which

the film is prepared (e.g., by first abrading the electrode surface with sand paper or alumina). Film loss can thus differ from film to film, and will indeed appear to be contributing less when using an older film due to the exponential nature of the current loss we see and/or its experiment history (Armstrong et al., 2009).
(57) Armstrong, F. A.; Belsey, N. A.; Cracknell, J. A.; Goldet, G.; Parkin, A.; Reisner, E.; Vincent, K. A.; Wait, A. F. *Chem. Soc. Rev.* **2009**, *38*, 36−51.
(58) Lamle, S. E.; Vincent, K. A.; Halliwell, L. M.; Albracht, S. P. J.; Armstrong, F. A. *Dalton Trans.* **2003**, 4152−4157.
(59) Fourmond, V.; Infossi, P.; Giudici-Orticoni, M.-T.; Bertrand, P.; Leger, C. *J. Am. Chem. Soc.* **2010**, *132*, 4848−4857.
(60) We have previously shown that extended incubation under H_2 (∼40 h) at high temperature (37 °C) of as-isolated C19G/C120G is necessary to remove the Ni−A signals (Lukey et al., 2011) and because the enzyme deteriorates under such extreme conditions it was not feasible to activate the entire enzyme volume required for a full titration in order to remove Ni−A and observe the Ni−B signals exclusively.
(61) Roessler, M. M. PhD Thesis, University of Oxford, 2012.
(62) At 5 °C, E_{switch} is ∼+0.16 V for native Hyd-1 and the P242C and C19G/C120G variants. Were we to use an even slower scan rate than 0.1 mVs^{-1}, it is likely that E_{switch} would increase to a more positive potential, but such measurements are impractical. The value of ∼+0.16 V represents a lower limit of E_{switch} at 5 °C, assuming there is no change in the rate determining step between 5 and 30 °C.
(63) Unden, G. *Arch. Microbiol.* **1988**, *150*, 499−503.
(64) Nitschke, W.; Russell, M. *J. Mol. Evol.* **2009**, *69*, 481−496.
(65) Sleep, N. H.; Bird, D. K. *Philos. Trans. R. Soc. B: Biol. Sci.* **2008**, *363*, 2651−2664.
(66) Pandelia, M.-E.; Lubitz, W.; Nitschke, W. *Biochim. Acta: Bioenerg.* **2012**, *1817*, 1565−1575.
(67) Wood, P. M. *Biochem. J.* **1988**, *253*, 287−289.
(68) Garcin, E.; Vernede, X.; Hatchikian, E. C.; Volbeda, A.; Frey, M.; Fontecilla-Camps, J. C. *Structure* **1999**, *7*, 557−566.
(69) Teixeira, M.; Fauque, G.; Moura, I.; Lespinat, P. A.; Berlier, Y.; Prickril, B.; Peck, H. D.; Xavier, A. V.; Le Gall, J.; Moura, J. J. G. *Eur. J. Biochem.* **1987**, *167*, 47−58.
(70) Parkin, A.; Goldet, G.; Cavazza, C.; Fontecilla-Camps, J. C.; Armstrong, F. A. *J. Am. Chem. Soc.* **2008**, *130*, 13410−13416.
(71) Manodori, A.; Cecchini, G.; Schroder, I.; Gunsalus, R. P.; Werth, M. T.; Johnson, M. K. *Biochemistry* **1992**, *31*, 2703−2712.
(72) Bingemann, R.; Klein, A. *Eur. J. Biochem.* **2000**, *267*, 6612−6618.
(73) Larkin, M. A.; Blackshields, G.; Brown, N. P.; Chenna, R.; McGettigan, P. A.; McWilliam, H.; Valentin, F.; Wallace, I. M.; Wilm, A.; Lopez, R.; Thompson, J. D.; Gibson, T. J.; Higgins, D. G. *Bioinformatics* **2007**, *23*, 2947−2948.
(74) Pandelia, M.-E.; Infossi, P.; Stein, M.; Giudici-Orticoni, M.-T.; Lubitz, W. *Chem. Commun.* **2012**, *48*, 823−825.
(75) Horch, M.; Lauterbach, L.; Saggu, M.; Hildebrandt, P.; Lendzian, F.; Bittl, R.; Lenz, O.; Zebger, I. *Angew. Chem., Int. Ed.* **2010**, *49*, 8026−8029.
(76) Pandelia, M.-E.; Fourmond, V.; Tron-Infossi, P.; Lojou, E.; Bertrand, P.; Léger, C.; Giudici-Orticoni, M.-T. r. s.; Lubitz, W. *J. Am. Chem. Soc.* **2010**, *132*, 6991−7004.